American Mineralogist, Volume 90, pages 1270–1277, 2005

TEM-specimen preparation of cell/mineral interfaces by Focused Ion Beam milling

MARTIN OBST,[1,*] PHILIPPE GASSER,[2] DENIS MAVROCORDATOS,[†,3] AND MARIA DITTRICH[1]

[1]Limnological Research Center, Swiss Federal Institute for Environmental Science and Technology (EAWAG), Seestrasse 79, CH 6047 Kastanienbaum, Switzerland
[2]Swiss Federal Laboratories for Materials Testing and Research (EMPA), CH 6800 Dübendorf, Switzerland
[3]Swiss Federal Institute for Environmental Science and Technology (EAWAG), CH 6800 Dübendorf, Switzerland

ABSTRACT

Picocyanobacteria were found to play an important role in calcite precipitation in oligotrophic lakes. In this study, investigations on the interface between cyanobacteria and attached biogenic calcite crystals have been performed to gain further insights into the mechanisms of nucleation of these precipitates. Ultramicrotomy, the conventional preparation technique of thin sections for Transmission Electron Microscopy (TEM) investigations, often fails when working on heterogeneous samples containing soft organic material and hard minerals. Thus, in this study the thin sections were prepared using Focused Ion Beam (FIB) milling. This approach is usually applied in material sciences but until recently was not very common in environmental research. Different analytical TEM methods like Electron Spectroscopic Imaging (ESI) and Electron Energy Loss Spectrometry (EELS) were used to test the suitability of FIB-milling for the preparation of organic/inorganic interface specimens. With this approach we were able to analyze both organic and the inorganic phases of the same sample. Elemental maps of the samples were also calculated. By analyzing the structure of the C *K*-absorption edge, the different bonding forms of the organic carbon cell and the inorganic carbon of the crystal could be clearly distinguished.

INTRODUCTION

Lacustrine calcite precipitation with sedimentation rates of several g/m^{2}d (calculated from Bloesch 1974) can result in large carbonate deposits. Varied lake sediments high in calcite content are now intensively studied as high-resolution continental archives for environmental change (Lotter et al. 1997). Eukaryotic and prokaryotic picoplankton species have been found to play an important role in the overall process of calcite precipitation, particularly in oligotrophic hardwater lakes.

Studies of biogenic calcite precipitation have been done from various perspectives. Several authors have analyzed environmental conditions leading to biogenic calcite precipitation (Canaveras et al. 2001; Merz-Preiss 2000; Castanier et al. 1999; Saiz-Jimenez 1999; Merz et al. 1995; Thompson and Ferris 1990; Thompson et al. 1997). Dittrich et al. (2004) combined field observations with laboratory experiments using several eukaryotic and prokaryotic plankton strains.

Besides these large-scale studies several microscopy studies have been performed. TEM investigations focused primarily on the paracrystalline proteinaceous surface layers (called S-layers) of cyanobacterial cells as a template for nucleation (Schultze-Lam and Beveridge 1994a, b; for review see Smarda et al. 2002). Schultze-Lam et al. (1992) suggest that as a first step hydrated Ca^{2+}-ions are bound to the regularly spaced and negatively charged proteins of the S-layer. These suggestions were based on structural investigations of S-layers and "bulk"-analysis of their chemical composition.

However, in our study we developed a sample preparation method for analytical TEM studies of thin sections of the interface between picoplankton cell walls and the crystals attached to these cells. Investigations of the C *K*-absorption edge by TEM-EELS provide information about the bonding of carbon at this interface and could therefore possibly prove the involvement of negatively charged proteins in the bonding of Ca^{2+} ions to the cell surface.

Conventionally thin sections of environmental samples for TEM investigations are cut using ultramicrotomy (e.g., Schultze-Lam et al. 1992). The heterogeneity of samples containing both soft organic material and hard minerals complicates the use of this conventional approach because minerals are barely cut by the diamond blade without applying stress to the interface between soft and hard matter. Another disadvantage of ultramicrotomy is the randomness of positioning of the slice plane. To overcome these limitations on investigations of heterogeneous cell-mineral interfaces, thin sectioning by Focused Ion Beam (FIB) milling has been successfully applied to environmental particles (Benzerara et al. 2005; Mavrocordatos et al. 2003; Heaney et al. 2001). These sections were prepared for analytical TEM studies.

Nevertheless, this technique has to be adapted to and optimized for heterogeneous samples containing both soft organic matter such as cyanobacterial cells and biogenic mineral phases. Mulders (2003) showed that it was possible to mill fragile organic matter. Using a cryo stage he was able to visualize the inner structure of cross-sectioned bacteria without any chemical fixation. However, from Mulders (2003) it is not clear if the physico-chemical structure of the milled side wall is affected by the FIB or preserved.

* E-mail: martin.obst@eawag.ch

0003-004X/05/0809–1270$05.00/DOI: 10.2138/am.2005.1743

In the current study the preparation of thin sections of cell/mineral-interfaces by FIB-milling was tested for its suitability by analytical TEM. Biogenic calcite crystals attached to *Synechococcus* cells were sectioned and analyzed with the intention of finding an appropriate preparation technique for high-resolution investigations at the interface. Elemental maps were measured by TEM-ESI and the carbon *K*-edge of both the mineral and crystal were analyzed by TEM-EELS. Our results therefore provide information on the suitability of the FIB-milling technique for TEM specimen preparation of delicate samples for environmental research.

Experimental details

Cultures

To control the optimum growth phase of the cyanobacteria, continuous cultures were used. Cyanobacteria of the *Synechococcus* strain PCC 7942 [Collection Nationale de Cultures de Microorganismes (CNCM), Institut Pasteur, Paris] were cultured in closed 2.5 l chemostats on Z/10 culture medium [5.9 mg/L $Ca(NO_3)_2 \cdot 4H_2O$, 46.7 mg/L $NaNO_3$, 4.1 mg/L $K_2HPO_4 \cdot 3H_2O$, 2.5 mg/L $MgSO_4 \cdot 7H_2O$, 168 mg/L $NaHCO_3$, 11.45 mg/L Na-EDTA, 3 mg/L $FeSO_4 \cdot 7H_2O$, H_3BO_3 248 µg/L, $MnSO_4 \cdot H_2O$ 135 µg/L, $(NH_4)_6Mo_7O_{24} \cdot 4H_2O$ 7,2 µg/L, $ZnSO_4 \cdot 7H_2O$ 23,2 µg/L, $Co(NO_3)_2 \cdot 6H_2O$ 12 µg/L, $CuSO_4 \cdot 5H_2O$ 10,4 µg/L] without vitamin solution. Culture medium was added by a peristaltic pump with a flow rate of 0.2 L/d through a sterile inlet. The bioreactors were aerated with sterile-filtered air. The pH of the cell suspension was measured with long-term stable combination electrodes (Mettler Toledo InPro 3030). To optimize growth conditions CO_2 was added to the aeration-air in case the pH rose above a maximum value of 7.5. The cultures were maintained at a temperature of 27 °C. Fluorescent lights provided a permanent light intensity of 7 µE/m^{2}s.

Cells were harvested for experiments upon reaching a stationary phase 3 weeks after activating the chemostats. The cells were centrifuged at 2000 g for 60 min, decanted, resuspended with Nanopure water, and centrifuged again for 30 minutes. This washing procedure was repeated twice before redispensing the cells. Depending upon the cell numbers of the concentrated suspensions several ml of these were added to the precipitation reactors after an initial equilibration phase, as described below, to reach a cell number of $1.0–1.5 \cdot 10^9$/L in the precipitation experiments.

Preparation of the supersaturated solutions

Bicarbonate and $CaCl_2$ solutions were prepared from reagent-grade chemicals (Fluka p.a.) and Nanopure water. The experiment was performed at a 1 mM $NaHCO_3$ concentration. A volume of 700 mL of the bicarbonate solution was poured into the reactor and equilibrated with 0.2 µm filtered ambient air. This procedure was performed by bubbling the solution through syringe needles.

Precipitation experiments

After an equilibration time of 1–2 h the data acquisition system started and the $CaCl_2$-solution was added by a peristaltic pump resulting in a 39 mM total Ca^{2+} concentration. To prevent induction of precipitation during the addition, $CaCl_2$ solutions were pumped through needles directly into bicarbonate solutions while stirring. In the next step the cell suspensions were added directly into the solutions with syringes. The solution was bubbled with air as described before during the entire experiment. Full-spectrum fluorescent light provided a light intensity of 13 µE/m^{2}s at a color temperature of 5400 K. The saturation with respect to calcite was calculated from measured values of pH, Ca^{2+}, and alkalinity, using the equilibrium constants from Stumm and Morgan (1996). The initial value of 8.0 dropped down to 2.5 within 26 hours and reached 1.3 after 5 days. In another series of experiments with saturations greater than 6.0 precipitation usually took place within two days (data not shown here).

Data acquisition

Ion activities, electrical conductivity, and temperature in the precipitation reactors were monitored continuously. For pH measurements Mettler-Toledo InPro 3030 combination pH electrodes (new model 2003 with ceramic diaphragm) were used. Ca^{2+} and CO_3^{2-}-activities were measured with PCV-based liquid membrane ion-selective electrodes (Müller et al. 1998). Electrical conductivity and temperature were measured using a computer-controlled WTW Cond 340i conductivity meter in combination with an electrode switch for 4 WTW Tetracon 325 electrodes.

Specimen preparation and analysis

Sample filtration. When precipitation was detected by changes in the ion activities and electrical conductivity 2 mL aliquots were sampled with syringes and filtered with 0.2 µm Nucleopore polycarbonate membrane filters in Millipore Swinnex filter cartridges. The filters were rinsed with 2 mL of Nanopure water to remove readily soluble salts. Afterward they were dried immediately with a vacuum filtering apparatus and stored at a temperature of 4 °C.

Preparation of TEM Sections. Filtered suspensions of the cells and crystals were thin sectioned with an FIB. A similar milling procedure was described and illustrated in detail in Heaney et al. (2001). In the current study a FEI DB 235 Strata model working with a liquid Ga source at an acceleration voltage of 30 kV was used for sectioning. The filter specimens were first sputter-coated with a platinum layer. The thickness of the layer was approximately 15–20 nm. To protect the upper side of the TEM lamella from the milling Ga-ions an additional thick (~1 µm) organometallic Pt-layer, called "Pt-strap" in Heaney et al. (2001), was deposed onto the milling region prior to the sectioning. In our study trenches were first milled on each side of the strap with high current. For the following reduction of thickness of the remaining lamella, the current was reduced stepwise (5000 - 1000 - 300 - 100 - 30 pA). In addition, the milling depth of each trench was stepwise reduced toward the strap, resulting in a wedge-shaped lamella between the trenches. When milling of the overall shape of the section was finished, the side walls of the lamella were cleaned at a milling current of only 10 pA to preserve the fragile organic matter. Using this milling technique a lamella thickness of approximately 150 nm could be obtained at the upper end of the section (estimation from SEM measurements). At the lower end of the section a thickness of several hundreds of nm was left to stabilize the lamella. The lamella was undercut after tilting the sample and finally the connections to the rest of the filter were milled. The thin sections then were removed from the filters and placed on TEM grids using a Narishige micromanipulator (MMO-202 ND) under an optical microscope.

Preparation of SEM samples. Samples for SEM were prepared with the process described above but only one trench was milled into a cell lying upon the filter. One side of the trench was prepared for SEM analysis with a cleaning mill. Subsequently this side was analyzed with the electron beam of the Dual-Beam FIB. Acceleration voltages of 5 kV (Fig. 1a) and 10 kV (Fig. 1b, 2a, 2b) were applied. Images were acquired with a through-the-lens secondary electron detector. The samples were tilted by 52° at a free working distance of about 5 mm.

Assessment of the ion beam damage on the specimen. To estimate the beam damage of the FIB on the thin sections, the trajectories and the collision cascades were simulated using the Monte-Carlo approach of Ziegler (2003). The "Stopping and Range of Ions in Matter" (SRIM) code version 2003.20 was used for all calculations. The incident angle of the ion beam was calculated as 1° from the vertical axis. Specimen densities of 1 g/cm^3 for organic matter and 2.71 g/cm^3 for $CaCO_3$ were chosen. For modeling the damage cascades the displacement energies were assumed to be similar to the lowest bonding energies of concern (Table 1).

TEM and Analyses by Electron Energy Loss Spectroscopy (EELS). For all investigations carbon-coated 300 mesh copper TEM grids were used. The samples were observed with a Zeiss EM 912 Ω energy filter model transmission electron microscope. The microscope, equipped with a LaB_6 source, was operated at 120 kV, and the emission current was set to 2 µA. Both images and EEL spectra were recorded with a Proscan CCD camera (1024 HSC, 14 Bit, 2 MHz). Corrections for noise (by subtraction) and gain were made to the CCD camera prior to the measurements.

The thin sections were first scanned in ordinary TEM bright-field mode (exposure time 500 ms). Once the areas of interest were selected (within the center of the cell and the crystal, respectively) EEL spectra of both the carbon *K*-edge and calcium $L_{2,3}$-edge were recorded in EELS-spectrum mode. EEL-spectra were

Table 1. Assumed displacement energies for both organic matter and $CaCO_3$

Displacement energy	H	C	O	Ca
CH_2O / bonding energy	C-H 4.3 eV*	C-C 3.6 eV*	C-O 3.7 eV*	
$CaCO_3$ / bonding energy		C-O / C=O 5 eV*	C-O / C=O 5 eV*	lattice energy 30.2 eV†

* Adapted from Schwarzenbach et al. (2003).
† Adapted from Mandell and Rock (1998).

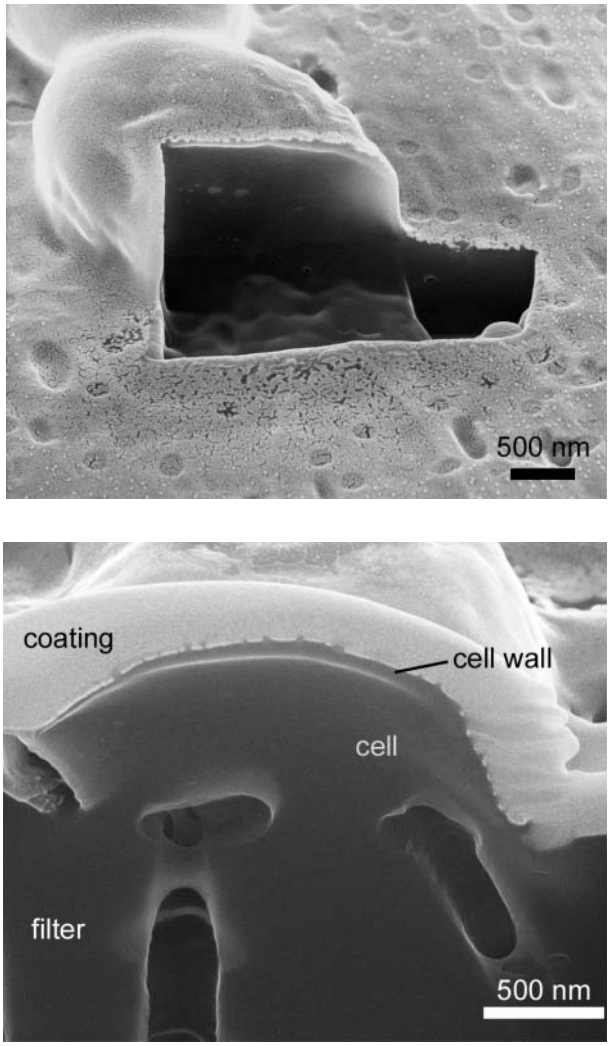

FIGURE 1. (**a**) SEM micrograph of an FIB-milled section of a *Synechococcus* cell lying on a polycarbonate filter; although no preservation technique but Pt-coating was applied prior to sectioning the cell did not collapse. (**b**) The cell wall of the same type of cell is not destroyed by the high energy Ga-ion beam in the FIB.

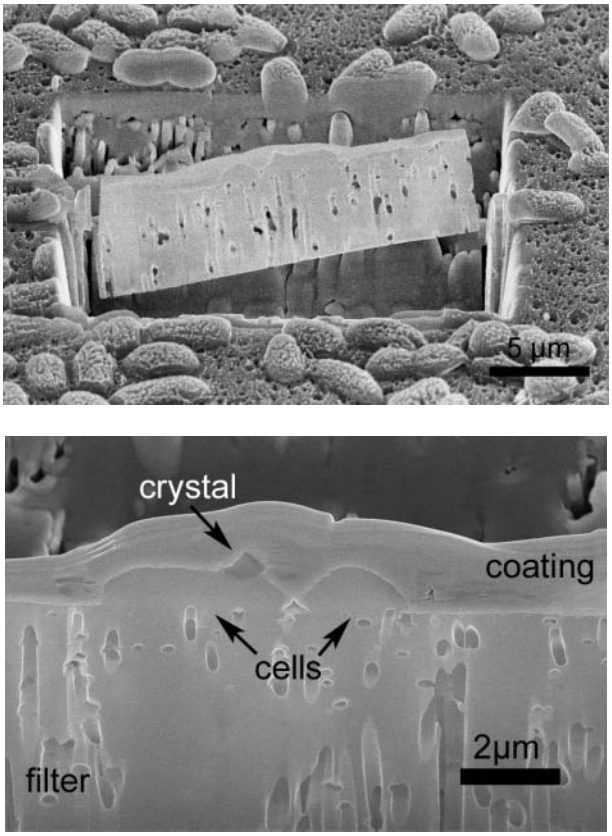

FIGURE 2. (**a**) Thin section preparation by FIB, ready to be deposited onto a TEM grid. (**b**) SEM image of the section at a higher magnification showing two cyanobacterial cells lying on a filter; a small calcite crystal is attached to one of the cells.

obtained at a magnification of 20 000 times over an integration time of 5000 msec. The C *K* and Ca $L_{2,3}$ edges were observed at 284 and 346 eV respectively.

The energy windows for the EEL spectra were set from 270–330 eV observing the C *K*-edge and 335–395 eV for the Ca $L_{2,3}$-edge to have a background fitting window prior to the ionization edge onsets. At a resolution of 1024 pixels for this energy range this setup had an equivalent energy dispersion of 0.06 eV per channel. Gray values of the spectra were measured and transformed using AnalySIS 3.0 (Soft Imaging System GmbH, Muenster, Germany). The spectral data were baseline-corrected. In high-loss regions where single electron excitation is the dominant process an approximately linear relationship was found between the logarithm of the intensity and the logarithm of the energy loss (Brydson 2001). Therefore the background could be fitted using the power law function:

$$I = A \cdot E^{-r} \tag{1}$$

where I is the signal intensity, E is the energy loss, and A and r are the fitting parameters. These parameters were determined by a linear least-squares fit in an energy window of 15 eV directly prior to the onsets of the ionization edges. The resulting background was extrapolated under the edge and subtracted from the signal.

Possibly due to the specimen thickness and the density of the calcite crystal, the signal to noise ratio was quite small for the C-edge recorded from the crystal, and three spectra were recorded for the same area with an energy-displacement of 1 eV. The resulting data were superimposed, summed up, and the resulting data background-corrected as described above.

The peaks of the spectra were fitted using an overlay of Gaussian peak functions:

$$y = \frac{A}{sd \cdot \sqrt{2 \cdot \pi}} \cdot e^{-\frac{(x-rt)^2}{2 \cdot sd^2}} \tag{2}$$

where A is the peak area, sd is the standard deviation, and rt is the energy loss of the peak maximum.

TEM electron spectroscopic imaging (ESI). Calcium, carbon, and oxygen elemental maps were obtained in ESI-mode with the same microscope as described above. The three window method described by Brydson (2001) was applied to calculate the elemental maps. The energy windows were set to $\delta W = 20$ eV. Two pre-edge images were used to fit the background (Eq. 1), which was extrapolated under the edge and subtracted from the core-edge intensities.

The acquisition times of 2 (C *K*-edge) and 5 sec (Ca $L_{2,3}$-edge and O *K*-edge) allowed the elemental maps to be recorded without specimen drift. The images were recorded at the following energy loss sequences: C *K*-edge, 237, 268, and 303 eV; Ca $L_{2,3}$-edge, 309, 332, and 357 eV; O *K*-edge, 493, 520, and 548 eV. These values are centered in the energy windows δW.

The thickness of the specimen was too large compared to the mean free path of plasmon losses (Reimer 1995). No deconvolution could be applied to eliminate multi-scattering effects (e.g., by the Fourier-Ratio method) because these techniques require that the whole energy loss spectrum be recorded.

RESULTS

Sample preparation

In a first experiment, cyanobacterial cells filtered from a cell suspension were cut by FIB while an organometallic Pt-coating preserved the outer morphological coarse structure of the cell. As shown by SEM in Figure 1a, the shape of the cell was protected from the high energy of the ion beam milling into the specimen. The cell did not collapse even though water was not substituted and the cell was not embedded in resin prior to the sectioning. Figure 1b shows the cell wall of *Synechococcus*. Structural details, however, could not be found by SEM after FIB-milling into this non-resin-embedded prokaryotic cell.

Figure 2a shows an SEM top view of the sectioned filter. After milling trenches in front and back of the region of interest, the thickness of the section was further reduced. Finally the specimen was tilted and the base was milled out. At this point the specimen was ready to be separated and deposited onto a TEM grid. The material was mechanically weak and therefore needed to be removed with great care. An SEM micrograph of the thin section is shown in Figure 2b. The relatively thick (~1 μm) organometallic Pt-strap, deposited onto the filter prior to FIB-milling, protected the soft organic material and the interface between cell and crystal from the high energy of the ion beam. Thus, the area of interest was less affected by milling Ga-ions.

TEM and TEM-ESI

Figure 3 shows an inverse TEM micrograph of a calcite crystal attached to a cyanobacterial cell. The cell-crystal interface appears sharp.

The same area as in the bright-field image is shown on elemental maps for calcium (Fig. 4a), carbon (Fig. 4b), and oxygen (Fig. 4c). Cell and crystal material clearly differ in elemental composition. Calcium is concentrated in the crystal, whereas the cell material only shows a weak calcium signal. The carbon signal of the cell material is stronger than observed in the crystal, whereas the oxygen signal is slightly more pronounced in the crystal. The elemental maps only show relative concentrations. Due to the specimen thickness no absolute measurements could be performed.

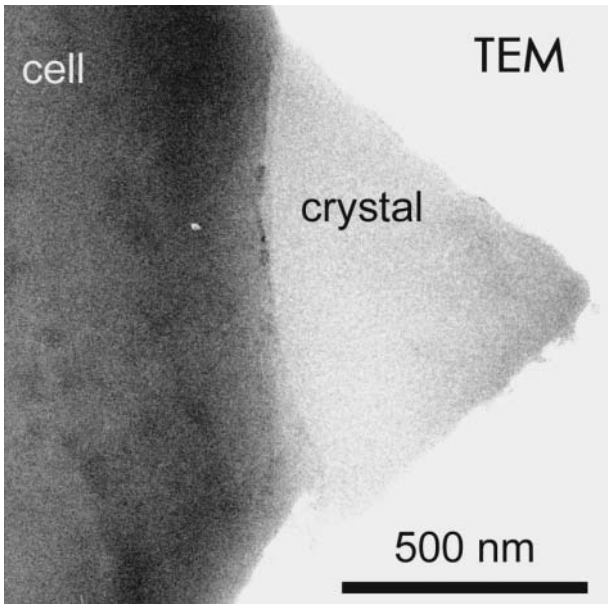

FIGURE 3. (**a**) Inverse TEM-micrograph of a calcite crystal precipitated onto the surface of a cyanobacterial cell.

TEM-EELS

Figure 5 shows the C *K*-absorption edge of both the cell and the crystal, and additionally the Ca $L_{2,3}$-edge of the crystal. The Ca signal of the cell could not be detected. The fitted curves of the C *K*-edge of the crystal clearly shows peaks at the following

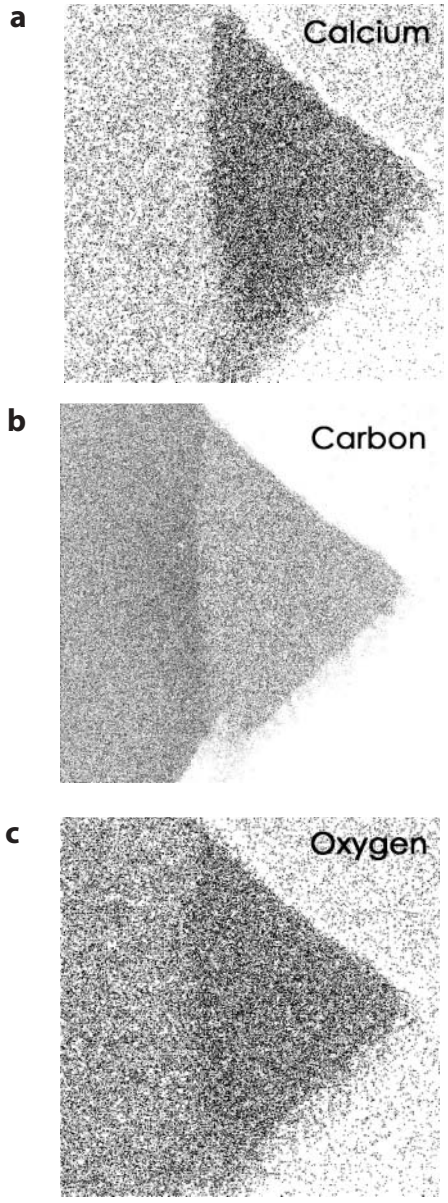

FIGURE 4. (**a**) Calcium $L_{2,3}$-edge image of the crystal attached to a *Synechococcus* cell; (**b**) carbon *K*-edge image; (**c**) oxygen *K*-edge image.

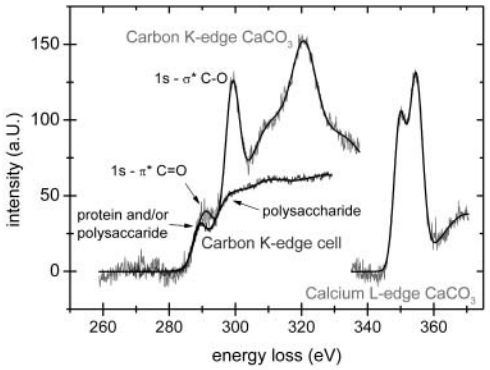

FIGURE 5. EEL spectra of the carbon *K*-edge of a cyanobacterial cell, an attached biogenic calcite crystal, and of the Ca $L_{2,3}$-edge of the crystal.

centers: 290.7 (1s/π*, C = O), 299.1 (1s/σ*, C-O), 309.3, 320.8, and 330.6 eV. The C *K*-edge of the cell only shows peaks at 288.8 (proteins and/or polysaccharides), 296.8 (polysaccharides), 306.9, and 328.5 eV. The peak maxima for the Ca $L_{2,3}$-edge of the crystal were detected at 349.7, 354.6, and 370.2 eV.

DISCUSSION

TEM is a useful tool for investigations of interfaces between biological surfaces and inorganic crystalline materials to understand the interaction between cell surfaces and the attached matter. Interfaces between cells and minerals are objects of investigations in many areas of science, for example, the study of biomineralization or the interaction of biomaterials and living cells in medical science.

Mavrocordatos and Fortin (2002) used analytical TEM methods to investigate the morphology and mineralogical and stoichiometric composition of synthetic biotic hydrous ferric oxid particles which formed in the presence of *Bacillus subtilis* and *Bacillus licheniformis*. Phoenix et al. (2000) used TEM to observe that mineralization of the cyanobacterium *Calothrix sp*. in silica and iron-silica solutions was mainly restricted to the outer surface of the cell sheaths. Konhauser and Urrutia (1999) investigated the mechanisms of biomineralization of (Fe, Al)-silicates on freshwater biofilms and cultured bacteria by means of TEM. They could explain the mechanism of nucleation by adsorption of cationic iron or colloidal species. Hofman et al. (1999) observed indications of bioactivity investigating the ultrastructure of rat-bone/biomaterial interfaces by TEM. Arp et al. (1999) investigated the calcification of cyanobacteria and their extracellular polymeric substances. In TEM-sections they observed accumulations of osmiophilic mucus substances surrounding the crystal traces. Schultze-Lam and Beveridge (1994a, b) and Schultze-Lam et al. (1992) performed detailed TEM studies of the role of cyanobacterial S-layers in biomineral nucleation.

In our field of study, analytical TEM will provide important information about the thickness and morphology of the interface between calcite crystals grown on the surface of cyanobacteria. Furthermore, measurements of the electron energy loss provide information on the chemical bonding forms of the specimen. These data are necessary to clarify the importance of possible mechanisms leading to the biomineralization of calcite.

However, one fundamental limiting factor of high-resolution analytical TEM measurements is the quality of the investigated thin section. Ultramicrotomy after high-pressure freezing and freeze substitution is the method of choice for structural investigations of biological samples embedded in resin (Walther and Muller 1999; Hesse and Hess 1994; Epperlein et al. 1997; Hohenberg et al. 1994). This method, however, has two mayor disadvantages with respect to our experiments. Firstly, because of the large difference in stiffness, the interface between the soft cell and the hard mineral could suffer from sheer stress applied by the cutting procedure with the diamond knife. Secondly, for ultramicrotomy the sample has to be embedded in resin. Therefore one is not able to choose the slice plane accurately perpendicular to the cell-mineral interface. Thus the thickness of this interface layer, observed by TEM, could be misinterpreted.

Evaluation of the FIB-milling procedure

Against this background FIB-milling was tested for preparation of TEM specimen that prior to this were rarely used in environmental research (e.g., Heaney et al. 2001; Shukla et al. 2001; Kim and Dravid 2000). The high energy of an incident ion beam provides sublimation of the material processed and therefore enables one to cut minerals (Mavrocordatos et al. 2003). Furthermore this technique offers the possibility of positioning the slice plane accurately because of the SEM environment when using a Dual-Beam-FIB. Thus, FIB-sectioning could be of general interest for investigations on inorganic/organic interfaces.

Our approach enabled us to cut thin sections across the cell-mineral interface of biogenic calcite. These sections were prepared on a conventional polycarbonate filter. An advantage of this approach is the possibility of preparing specimens of interfaces between cells and relatively insoluble minerals such as $CaCO_3$. Highly soluble salts, contaminating the sample, can be removed by purified water. The sample has to be dried immediately after this washing step in order not to dissolve the biomineral. This technique can also be used for cleaning environmental samples.

However, two mayor disadvantages limit our approach: Firstly, the inner structure of the cells is not well preserved because of air-drying the samples prior to thin sectioning. Thus this method should not be used for structural investigations on the cell itself.

Secondly, the key limitation of the FIB approach is the optimization of the milling technique and the energy of the incident ion beam. As shown by Mulders (2003) it is possible to FIB-mill organic specimens and preserve the structure of the fragile matter. However, more difficulties will occur when milling into specimens containing both organic matter and minerals. Whereas milling minerals requires high currents of the FIB to limit the milling time, the high energy damages the structure of the cells. An optimum energy has to be found to be able to cut the mineral phase, but preserve the fragile organic material.

This problem was handled in a way similar to the approach of Smith et al. (2001). After initial "large mills" the thickness of the section was reduced by "cleaning mills". For these cleaning mills the beam current was reduced in succession, to reduce the beam damage on the area of interest.

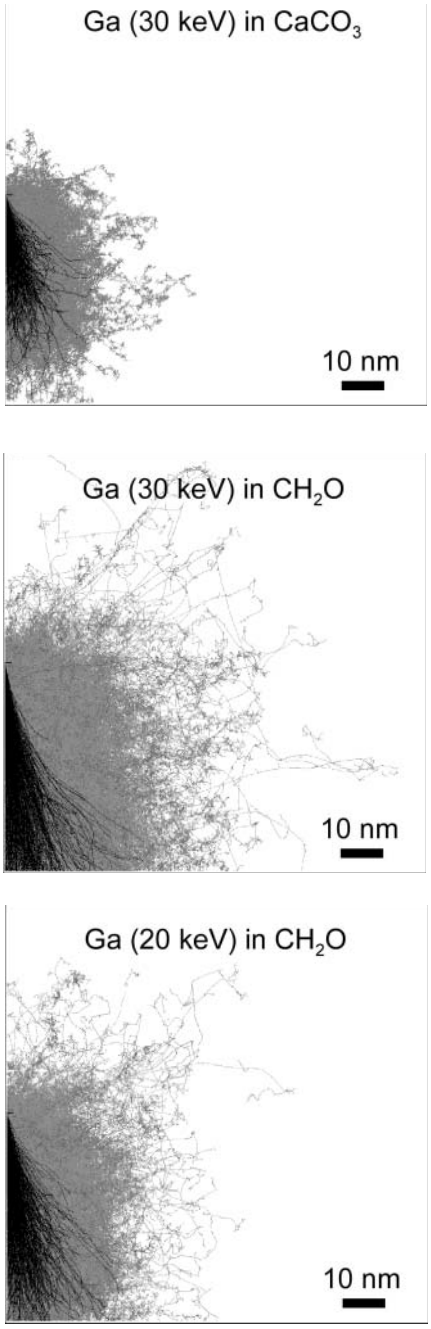

FIGURE 6. Monte-Carlo simulations of the Ga-ion trajectories (black) and the full cascades of energy loss (grey) calculated with the SRIM 2003 code in organic matter of composition CH_2O (**a**) and in $CaCO_3$ (**b**). The beam hits the specimen in the center of the left border at an angle of incidence of 1° from upside down. In comparison to a 30 keV Ga beam used for the simulations described above, (**c**) illustrates the same simulation in CH_2O for 20 keV Ga ions.

The sections shown in Figures 1a and 1b clearly demonstrate that sputter coating the specimen with a Pt-layer and covering the desired section with a Pt-strap prior to FIB-milling produces optimal results when combined with careful milling. Our results then correspond with the findings of Benzerara et al. (2005) and Mulders (2003). Although the cyanobacterial cells were not embedded in resin, the coarse morphology and outer shape was barely damaged by the preparation technique.

Modeling-beam damage

However, the influence of the incident high-energy ion beam on the morphological fine structure of the remaining cell wall is not clear. Furthermore, artifacts produced by the high-energy Ga ions have to be considered. The upper side of the sample can be well protected by sputter-coating the sample with platinum. Thus more attention should be addressed to the sidewall beam damage by low-angle incident ions. For estimation of the range of this beam damage on the sample the Monte-Carlo approach of "Stopping and Range of Ions in Matter" (SRIM) of Ziegler (1998), based on principles of quantum mechanics, was found to be useful by Orloff et al. (2003). In this approach penetration of the ions into matter is simulated three dimensionally by this approach. A full description of the calculations is given in Ziegler et al. (1985).

Kim and Dravid (2000) modeled the trajectories of 30 keV incident Ga-ions in Al_2O_3 and $CaWO_4$ using the routines written by Ziegler (1998). The thickness of the influenced and damaged sidewall layer was estimated to be, at most, 20 nm per side. McCaffrey et al. (2001) determined a similar thickness of the damaged layer for a 50 keV Ga ion beam when milling into silicon (30 nm).

As the energy necessary for displacement of target atoms is lower for amorphous organic matter (see Table 1), and mainly because the density of organic matter is much less than that of crystalline material, the range of low-angle incident ions is higher in biological samples. Figure 6b shows the simulation of ion trajectories and the full cascades of energy loss of 30 keV Ga ions penetrating into organic matter with the general composition of CH_2O. For each plot 1000 incident ions were modeled at an incident angle of 1° from the vertical axis. These ions hit the specimen at the center of the left side of the two-dimensional projection. The simulation takes all recoils of the following collisions into account. Figure 6a illustrates the range of Ga and following damage to $CaCO_3$. However, for crystalline material one has to consider that this model treats the specimen as amorphous with atoms at random locations. The orientation and anisotropic lattice properties of the calcite crystals do not play a role in the simulation. Therefore, in the case of the crystalline specimen the simulations represent only a coarse approximation.

In organic matter the range of the beam damage was approximately 40–50 nm whereas the damage in $CaCO_3$ was restricted to 20–30 nm. From these results it can be assumed that a certain fraction of the TEM-lamella may loose its original structure, but in the central part of the ~150 nm thick section the matter is not directly influenced by the milling procedure.

The milling process can be optimized using different acceleration voltages for the ion beam. Figure 6c illustrates the same simulation as Figure 6a but 20 keV ions are penetrating the specimen. The size of damaged cross-section is obviously less (about 30 nm) compared to the 30 keV simulation, but one has to take into account that lower beam energies implies necessarily longer milling times and therefore a higher number of incident

ions. Therefore we suggest an optimum combination of beam energy and milling time. As this optimum is difficult to access by a modeling approach, comparative and quantitative studies on the sidewall beam damage with similar approaches as discussed below could help to optimize thin sectioning of organic matter with an FIB.

Discussion of TEM results

The side-wall beam damage estimated above should be considered for interpreting the results of our TEM-investigations. As shown in Figures 4a-c investigations on the elemental composition by TEM-ESI were possible with our thin section. However, for quantitative and high-resolution measurements the specimen thickness and therefore also the thickness of the damaged sidewall layers should be further reduced. A specimen thickness of 100 nm or less with minimum beam damage would be optimal for our measurements. However, the specimen thickness reduction is limited by the mechanical stability of the section which can be improved by milling a wedge-shaped thin section instead of a parallel-shaped one.

TEM-EELS provides information about the bonding form of the carbon. In a further study these measurements should be performed with nanometer resolution to analyze the boundary layer between cell and crystal in detail. In this preliminary study the difference of the C *K*-edges of the organic and inorganic carbon could clearly be distinguished. Details of the carbon edge were observed and the absorption edges could be well fitted. The observed peak maxima for $CaCO_3$ are nearly the same as the values observed by Martin et al. (1989) by TEM-EELS. Both $CaCO_3$ and organic carbon peaks of the current study nearly coincide with the results Lawrence et al. (2003) obtained by near-edge X-ray absorption spectroscopy (NEXAFS) of the carbon edges of several reference compounds including polysaccharide (sodium alginate), protein (albumin), and $CaCO_3$. Nevertheless, from the results observed in our study it is not clear if the fine structure of the absorption edge is influenced by the FIB-milling or well preserved from the high energy of the incident ion beam.

Thus, a comparative EELS-study of specimen preparation by FIB-milling and ultramicrotomy should be done as the next step to prove the suitability of this preparation technique for quantitative investigations on cell-mineral interfaces. Furthermore, it should be tested if both morphology and fine structure of cells and organelles are preserved, by FIB-cutting thin sections of high-pressure freeze-substituted samples embedded in resin.

To prove the importance of S-layer proteins on the cell surface another EELS-study should be performed across the cell-mineral interface at high spatial resolution.

The results shown in this study demonstrate the possibilities of TEM specimen preparation of cell-mineral interfaces by FIB-milling. After further optimization of the milling technique FIB milled thin sections seem to be suitable for detailed microanalysis by analytical TEM. As it is possible to cut hard mineral phases this method is superior to conventional approaches. Working with a Dual-Beam-FIB further enables one to choose single particles of interest for the investigations. Thus it is possible to effectively process filtered laboratory or even environmental samples without extensive sample preparation.

However, possible artifacts produced by this approach have to be considered. Estimating the beam damage on the specimen with SRIM may be an effective tool for improving and optimizing the experiment. Nevertheless to find the optimum combination of beam energy and milling time further detailed and quantitative studies need to be performed.

ACKNOWLEDGMENTS

The authors thank M. Müller, Swiss Federal Institute for Science and Technology, Institute for Applied Physics, for TEM access and for helpful comments and discussion of the results and B. Wehrli for support and critical discussion of the manuscript. This study was supported by an ETH research grant (0-20967-02). Critical and constructive comments from the reviewers helped improve this paper.

This paper is dedicated to Denis Mavrocordatos, who had a fatal sailing accident before this study was finished. We continued this work in remembrance of an enthusiastic scientist and good friend.

REFERENCES CITED

Arp, G., Thiel, V., Reimer, A., Michaelis, W., and Reitner, J. (1999) Biofilm exopolymers control microbialite formation at thermal springs discharging into the alkaline Pyramid Lake, Nevada, USA. Sedimentary Geology, 126, 159–176.

Benzerara, K., Menguy, N., Guyot, F., Vanni, C., and Gillet, P. (2005) TEM study of a silicate-carbonate-microbe interface prepared by focused ion beam milling. Geochimica Et Cosmochimica Acta, 69(6), 1413–1422.

Bloesch, J. (1974) Sedimentation und Phosphorhaushalt im Vierwaldstättersee (Horwer Bucht) und im Rotsee. Schweizerische Zeitschrift für Hydrologie, 36, 71–186.

Brydson, R. (2001) Electron Energy Loss Spectroscopy, 137 p. BIOS Scientific Publishers Ltd., Oxford, Oxford, U.K.

Canaveras, J.C., Sanchez-Moral, S., Soler, V., and Saiz-Jimenez, C. (2001) Microorganisms and microbially induced fabrics in cave walls. Geomicrobiology Journal, 18, 223–240.

Castanier, S., Le Metayer-Levrel, G., and Perthuisot, J.P. (1999) Ca-carbonates precipitation and limestone genesis - the microbiogeologist point of view. Sedimentary Geology, 126, 9–23.

Dittrich, M., Kurz, P., and Wehrli, B. (2004) The role of autotrophic picocyanobacteria in calcite precipitation in an oligotrophic lake. Geomicrobiology Journal, 21, 45–53.

Epperlein, H.H., Schwarz, H., Piendl, T., Lofberg, J., Studer, D., Spring, H., and Muller, M. (1997) Improved preservation of the subepidermal extracellular matrix in axolotl embryos using electron microscopical techniques based on cryoimmobilization. Journal of Structural Biology, 118, 43–61.

Heaney, P.J., Vicenzi, E.P., Giannuzzi, L.A., and Livi, K.J.T. (2001) Focused ion beam milling: A method of site-specific sample extraction for microanalysis of Earth and planetary materials. American Mineralogist, 86, 1094–1099.

Hesse, M. and Hess, M.W. (1994) Recent trends in tapetum research - a cytological and methodological review. In M. Hesse, E. Pacini, and M.T.M. Willemse, Eds., The Tapetum: Cytology, Function, Biochemistry and Evolution. Plant Systematics and Evolution, Supplement 7. Springer, New York.

Hofman, S., Sidqui, M., Abensur, D., Valentini, P., and Missika, P. (1999) Effects of Laddec (R) on the formation of calcified bone matrix in rat calvariae cells culture. Biomaterials, 20, 1155–1166.

Hohenberg, H., Mannweiler, K., and Muller, M. (1994) High-pressure freezing of cell-suspensions in cellulose capillary tubes. Journal of Microscopy-Oxford, 175, 34–43.

Kim, S.T. and Dravid, V.P. (2000) Focused ion beam sample preparation of continuous fibre- reinforced ceramic composite specimens for transmission electron microscopy. Journal of Microscopy-Oxford, 198, 124–133.

Konhauser, K.O. and Urrutia, M.M. (1999) Bacterial clay authigenesis: a common biogeochemical process. Chemical Geology, 161, 399–413.

Lawrence, J.R., Swerhone, G.D.W., Leppard, G.G., Araki, T., Zhang, X., West, M.M., and Hitchcock, A.P. (2003) Scanning transmission X-ray, laser scanning, and transmission electron microscopy mapping of the exopolymeric matrix of microbial biofilms. Applied and Environmental Microbiology, 69, 5543–5554.

Lotter, A.F., Sturm, M., Teranes, J.L., and Wehrli, B. (1997) Varve formation since 1885 and high-resolution varve analyses in hypertrophic Baldeggersee (Switzerland). Aquatic Sciences, 59, 304–325.

Mandell, G.K. and Rock, P.A. (1998) Lattice energies of calcite-structure metal carbonates - II. Results for $CaCO_3$, $CdCO_3$, $FeCO_3$, $MgCO_3$, and $MnCO_3$. Journal of Physics and Chemistry of Solids, 59, 703–712.

Martin, J.M., Mansot, J.L., and Hallouis, M. (1989) Energy Filtered Electron-Microscopy (EFEM) of overbased reverse micelles. Ultramicroscopy, 30, 321–327.

Mavrocordatos, D. and Fortin, D. (2002) Quantitative characterization of biotic iron oxides by analytical electron microscopy. American Mineralogist, 87, 940–946.

Mavrocordatos, D., Steiner, M., and Boller, M. (2003) Analytical electron microscopy and focused ion beam: complementary tool for the imaging of copper sorption onto iron oxide aggregates. Journal of Microscopy-Oxford, 210, 45–52.

McCaffrey, J.P., Phaneuf, M.W., and Madsen, L.D. (2001) Surface damage formation during ion-beam thinning of samples for transmission electron microscopy. Ultramicroscopy, 87, 97–104.

Merz, M., Schlue, W.R., and Zankl, H. (1995) pH-Measurements in the Sheath of Calcifying Filamentous Cyanobacteria. Bulletin de l' Institut Océanographique, Monaco, Spécial 14, 283–289.

Merz-Preiss, M. (2000) Calcification in cyanobacteria. In R.E. Riding and S.M. Awramik, Eds., Microbial Sediments, p. 50–56. Springer Verlag, Berlin, Heidelberg, New York, Berlin, Heidelberg, New York.

Mulders, H. (2003) The use of a SEM/FIB DualBeam applied to biological Samples. Imaging and Microscopy, 5, 8–10.

Müller, B., Buis, K., Stierli, R., and Wehrli, B. (1998) High spatial resolution measurements in lake sediments with PVC based liquid membrane ion-selective electrodes. Limnology and Oceanography, 43, 1728–1733.

Orloff, J., Utlaut, M., and Swanson, L. (2003) High resolution focused ion beams: FIB and its applications the physics of liquid metal ion sources and ion optics and their application to focused ion beam technology. 303 p. Kluwer Academic/ Plenum Publishers, New York.

Phoenix, V.R., Adams, D.G., and Konhauser, K.O. (2000) Cyanobacterial viability during hydrothermal biomineralisation. Chemical Geology, 169, 329–338.

Reimer, L. (1995) Electron Spectroscopic Imaging. In L. Reimer, Ed., Energy-filtering transmission electron microscopy, 71, 347–400. Springer, Berlin etc.

Saiz-Jimenez, C. (1999) Biogeochemistry of weathering processes in monuments. Geomicrobiology Journal, 16, 27–37.

Schultze-Lam, S. and Beveridge, T.J. (1994a) Physicochemical characteristics of the mineral-forming S-layer from the Cyanobacterium Synechococcus strain Gl24. Canadian Journal of Microbiology, 40, 216–223.

——— (1994b) Nucleation of celestite and strontianite on a Cyanobacterial S-layer. Applied and Environmental Microbiology, 60, 447–453.

Schultze-Lam, S., Harauz, G., and Beveridge, T.J. (1992) Participation of a Cyanobacterial-S Layer in fine-grain mineral formation. Journal of Bacteriology, 174, 7971–7981.

Schwarzenbach, R.P., Gschwend, P.M., and Imboden, D.M. (2003) Environmental Organic Chemistry, 1313 p. Wiley-Interscience, Hoboken, New Jersey.

Shukla, S., Seal, S., Akesson, J., Oder, R., Carter, R., and Rahman, Z. (2001) Study of mechanism of electroless copper coating of fly-ash cenosphere particles. Applied Surface Science, 181, 35–50.

Smarda, J., Smajs, D., Komrska, J., and Krzyzanek, V. (2002) S-layers on cell walls of cyanobacteria. Micron, 33, 257–277.

Smith, A.J., Munroe, P.R., Tran, T., and Wainwright, M.S. (2001) FIB preparation of a sensitive porous catalyst for TEM elemental mapping at high magnifications. Journal of Materials Science, 36, 3519–3524.

Stumm, W. and Morgan, J.J. (1996) Aquatic chemistry chemical equilibria and rates in natural waters. XVI, 1022 p. Wiley, New York.

Thompson, J.B. and Ferris, F.G. (1990) Cyanobacterial precipitation of gypsum, calcite, and magnesite from natural alkaline lake water. Geology, 18, 995–998.

Thompson, J.B., Schultze-Lam, S., Beveridge, T.J., and DesMarais, D.J. (1997) Whiting events: Biogenic origin due to the photosynthetic activity of cyanobacterial picoplankton. Limnology and Oceanography, 42, 133–141.

Walther, P. and Muller, M. (1999) Biological ultrastructure as revealed by high resolution cryo- SEM of block faces after cryo-sectioning. Journal of Microscopy-Oxford, 196, 279–287.

Ziegler, J.F. (1998) The stopping and range of ions in matter (SRIM - 2000). IBMresearch, Yorktown, N.Y.

——— (2003) The stopping and range of ions in matter (SRIM - 2003). Annapolis, Maryland. http://www.srim.org/SRIM/SRIM2003.htm.

Ziegler, J.F., Biersack, J.P., and Littmark, U. (1985) The stopping and range of ions in solids. 321 p. Pergamon Press, New York.

MANUSCRIPT RECEIVED JUNE 9, 2004
MANUSCRIPT ACCEPTED DECEMBER 8, 2004
MANUSCRIPT HANDLED BY BERTRAND DEVOUARD